# Comparative assessment of visible light and UV active photocatalysts by hydroxyl radical quantification

Nagarajan, S., Skillen, N. C., Fina, F., Zhang, G., Randhorn, C., Lawton, L. A., Irvine, J. T. S., & Robertson, P. K. J. (2017). Comparative assessment of visible light and UV active photocatalysts by hydroxyl radical quantification. *Journal of Photochemistry and Photobiology A: Chemistry*, *334*, 13-19. https://doi.org/10.1016/j.jphotochem.2016.10.034

## Published in:
Journal of Photochemistry and Photobiology A: Chemistry

## Document Version:
Peer reviewed version

## Queen's University Belfast - Research Portal:
Link to publication record in Queen's University Belfast Research Portal

1  **Comparative assessment of visible light and UV active photocatalysts by hydroxyl**

2  **radical quantification**

3  Sanjay Nagarajan[1]*, Nathan C. Skillen[1], Federica Fina[2], Guan Zhang[2], Chamnan

4  Randorn[2], Linda A. Lawton[3], John T.S. Irvine[2] and Peter K.J. Robertson[1]*

5  [1] Centre for the Theory and Application of Catalysis (CenTACat), School of Chemistry

6  and Chemical Engineering, Queen's University Belfast, David Keir Building, Stranmillis

7  Road, Belfast, BT9 5AG, United Kingdom;

8   [2] JTSI Group, University of St. Andrews, School of Chemistry, Purdie Building, North

9  Haugh, St Andrews, KY16 9ST, United Kingdom;

10  [3]School of Pharmacy and Life sciences, Sir Ian Wood Building

11  Robert Gordon University, Garthdee Road, Aberdeen, AB10 7GJ, United Kingdom

12  *Corresponding authors, *p.robertson@qub.ac.uk; snagarajan01@qub.ac.uk, Tel: +44*

13  *(0) 28 9097 4627*

14

15  **ABSTRACT**

16      A simple method for determining hydroxyl radical yields on semiconductor

17  photocatalysts is highly desirable, especially when comparing different photocatalyst

18  materials. This paper reports the screening of a selection of visible light active

19  photocatalysts such as $Pt-C_3N_4$, 5% LaCr doped $SrTiO_3$, $Sr_{0.95}Cr_{0.05}TiO_3$ and Yellow

20  $TiO_2$ and compares them against $WO_3$ and ultra violet (UV) light activated $TiO_2$ P25

21  (standard commercial catalysts) based on their oxidative strengths (OH radical

22  producing capability) using a well-studied chemical probe – coumarin. 7-

23  hydroxycoumarin, the only fluorescent hydroxylation product of this reaction can then

24  be measured to indirectly quantify the OH radicals produced. P25 under UV light

25  produced the highest concentration of OH radicals (16.9 µM), followed by $WO_3$ (0.56

26  µM) and $Pt-C_3N_4$ (0.25 µM). The maximum OH radical production rate for P25, $WO_3$

27 and Pt-C$_3$N$_4$ were also determined and found to be 35.6 µM/hr, 0.28 µM/hr and 0.88

28 µM/hr respectively. The other visible light activated photocatalysts did not produce any

29 OH radicals primarily as a result of their electronic structure. Furthermore, it was

30 concluded that, if any visible light absorbing photocatalysts are to be fabricated in

31 future for the purpose of photocatalytic oxidation, their OH radical producing rates (and

32 quantities) should be determined and compared to P25.

33 **Keywords:** Photocatalyst, visible light photocatalysts, OH radical, coumarin, P25.

34

35

36

37

38

39

40

41

42

43

44

45

46

47

48

49

## 1.  INTRODUCTION

Photocatalysis has gained significant interest since the early publication by Fujishima and Honda in 1972, demonstrating the potential of splitting water over $TiO_2$ [1]. Since this publication, photocatalysis has been applied to a broad range of fields including waste water treatment, microbe destruction, toxin removal, energy production and air treatment. [2-8]. The mechanism of photocatalysis has been well documented and can be generally represented by the equations shown in reactions 1-9 [9,10]. The formation of surface radical species such as superoxide ($O_2^{-}$) and hydroxyl radicals (OH·) play a key role in a number of photocatalytic pathways and as such their identification and quantification is a key consideration. As shown in reaction 2, OH radicals are primarily generated from the reaction between valence band holes ($h_{vb+}$) and hydroxyl ions on the catalyst surface. An indirect pathway, via $O_2^{-}$, also results in OH radical formation, as shown in reactions 3-6. The efficiency of OH radicals in photocatalytic reactions is predominantly based on their strong oxidising potential of 2.8 V (vs NHE) [11]. The non-selective nature of these reactive oxygen species also aids rapid degradation of various pollutants and organic contaminants [3,7,11-16].

$$Photocatalyst \ + h\nu \ \rightarrow \ \ h_{vb+} + e_{cb-} \ \text{.......................................................... (1)}$$

$$h_{vb+} + OH^-(or \ H_2O) \rightarrow OH· \ \text{.......................................................... (2)}$$

$$e_{cb-} + O_2 \rightarrow O_2^{-}· \ \text{.......................................................... (3)}$$

$$O_2^{-}· + H^+ \rightarrow HO_2' \ \text{.......................................................... (4)}$$

$$HO_2' + HO_2' \rightarrow H_2O_2 + O_2 \ \text{.......................................................... (5)}$$

$$H_2O_2 + e_{cb-} \rightarrow OH· + OH^- \ \text{.......................................................... (6)}$$

$$O_2^{-}· + reactants \rightarrow products \ \text{.......................................................... (7)}$$

$$substrates +· OH \rightarrow products \ \text{.......................................................... (8)}$$

75  $e_{cb^-} + OH^. \rightarrow OH^-$                                       ......................................................... (9)

76  where, $h_{vb}^+$ represents VB holes and $e_{cb}^-$ means CB electrons.

77

78      Newly developed photocatalytic technologies and materials have often utilised

79  model compounds and screening methods to assess their performance [17-20].

80  Common evaluation methods reported in the literature include the decomposition of

81  dyes such as methylene blue (ISO test 10678:2010), or degradation of organic

82  pollutants such as 4-chlorophenol or toluene [17-20]. These procedures are often

83  coupled with the corresponding calculated photonic efficiencies and quantum yields to

84  evaluate overall efficiency. While these methods can be effective in identifying the

85  specific photocatalytic performance of a material in relation to a fingerprint compound,

86  they provide little information regarding the production of OH radicals involved within

87  the mechanism. Therefore, the requirement for a simple and robust method of radical

88  quantification for screening the oxidative potential of catalysts has significantly

89  increased. The challenge in OH radical quantification lies in both the non-selective

90  nature and short lifetime (~ 1 nanosecond) of the radical, which restricts the possibility

91  of direct quantification [21]. Consequently, a range of methods have been developed

92  such as emission spectroscopy, laser induced fluorescence, electron spin resonance,

93  spin trap and chemical probes or quencher based methods to quantify OH radicals [21-

94  37].

95

96      The use of a chemical probe to capture OH radicals presents a potentially efficient

97  way to measure the radical due to the low cost, rapid analysis time and reproducibility

98  of the method. Monitoring a probe compound through spectroscopy allows the

99  concentration of OH radicals to be calculated based on stoichiometric ratios of products

100 formed. A recently reported *in vivo* technique utilised a nanoprobe comprising of a

101 nanoparticle and azo dye in order to quantify OH radicals in the femtomolar range [37].

102 Here the nanoparticle was used as an energy donor and the modified orange was used

103 as an OH radical capturing ligand molecule (and the energy acceptor).

104

105     Dimethyl sulfoxide (DMSO) based methods for OH radical capture have also been

106 utilised in the past to quantify these species via the formation of formaldehyde

107 [28,29,31]. The formation of $CH_4$ in a closed system coupled with $O_2$ bubbling however

108 reduces the suitability of utilising DMSO as a probe molecule.

109

110     In the past, OH radical quantification has been carried out for various commercially

111 available photocatalysts, photo-Fenton's reaction and other modified $TiO_2$ based visible

112 light photocatalysts with either coumarin or terepthalic acid as probe molecules

113 [21,23,31-36,38,39]. Both compounds are capable of acting as OH radical traps by

114 forming fluorescent products as result of reacting with the radical species. Terepthalic

115 acid has been investigated in a study by Ishibashi *et al*. which achieved an OH radical

116 concentration of $7 \times 10^{-5}$ M based on the measurement of 2-hydroxyterepthalic acid

117 [35]. In addition to the use of terepthalic acid as a probe molecule, coumarin has been

118 used in a number of studies to determine the concentration of OH radicals produced

119 from $TiO_2$ at relatively high loadings of 1 to 5 g/L [21,23,40]. For instance, Czili *et al*.

120 used 100 µM coumarin as the probe molecule to capture OH radicals under a 40 W UV

121 lamp. They determined a maximum OH radical production rate of 23.39 µM/g/hr

122 (calculated from their reported 7-hydroxycoumarin rates) with 1 g/L $TiO_2$ P25

123 photocatalyst.

124

125     This paper utilises coumarin as a hydroxyl radical trap and reports the screening of

126 a selection of visible light responsive photocatalysts under low power illumination

127 based on their OH radical producing capability. In contrast to previous reports, which

128 concentrated on quantifying the OH radicals produced from $TiO_2$, other commercially

129 available and a few synthesised photocatalysts [21,23,31,40], this work focusses on

130 assessing the oxidative strength of visible light photocatalytsts Pt-$C_3N_4$, 5% LaCr

131 doped $SrTiO_3$, $Sr_{0.95}Cr_{0.05}TiO_3$ (referred to as Cr-$SrTiO_3$ from here on) and yellow $TiO_2$

132 and compares them against commercial $TiO_2$ P25 and $WO_3$ for evaluation. In addition,

133 a low catalyst loading was used to highlight efficient OH radical formation can be

134 achieved without requiring large quantities of powdered catalyst.

135

136 **2.   EXPERIMENTAL PROCEDURE**

137 **2.1  Materials**

138    Coumarin and 7-hydroxycoumarin were purchased from Tokyo Chemical Industry

139 UK Ltd, while $TiO_2$ P25 was purchased from Degussa (now Evonik industries) and $WO_3$

140 nano powders were purchased from Sigma Aldrich. All commercial chemicals were

141 used as received. The catalysts Pt-$C_3N_4$ [41], 5% LaCr doped $SrTiO_3$, Cr-$SrTiO_3$ and

142 yellow $TiO_2$ [42] were synthesised at the school of chemistry, University of St. Andrews,

143 using methods cited in the literature [41-43].

144

145 **2.2  Characterisation of Photocatalysts**

146    $WO_3$, LaCr-$SrTiO_3$ and Cr-$SrTiO_3$ were characterised by X-Ray diffraction (XRD)

147 and UV-Visible absorption. XRD analysis of powders was examined on a SToe

148 STADI/P powder diffractometer. Incident radiation was generated using a Cu $k_\alpha$ source

149 ($\lambda$=1.54056 Å). Diffuse reflectance spectra were collected on a JASCO-V550 UV-

150 visible spectrophotometer. The characterisation of Pt-$C_3N_4$ and yellow $TiO_2$ has been

151 reported elsewhere in literature [41,42].

152

153 **2.3  Photocatalytic experiments**

154    All photocatalytic experiments were performed in closed screw cap bottles. The

155 reaction solution was composed of 100 ml of 100 µM coumarin along with 10 mg of

6

156    photocatalyst (0.1 g/L). A magnetic stirrer bar was placed inside the bottle and the

157    bottle was then placed on a magnetic stirrer at a distance of 11 cm from a 36 W

158    compact fluorescent non-integrated visible lamp (Philips, colour code 830) or a 36 W

159    UV lamp (Philips, Cleo lamps). The spectral outputs of the lamps were measured by a

160    StellaNet spectrometer and the spectra are shown in the supplementary material

161    (Figure S1). Prior to illumination, the reaction solution was stirred in the dark to allow a

162    state of equilibrium to be reached. The length of time required in the dark was

163    calculated from the control experiments conducted in the absence of light. During

164    irradiation, samples (3 mL) were taken at dedicated time intervals for a maximum of

165    120 mins. Samples were filtered through a 0.22 μm Millex syringe filter prior to

166    analysis. Coumarin absorbance was monitored using a Cary 300 Scan, UV-Visible

167    Spectrophotometer at 277 nm, with a scan rate of 400 nm/min. 7-hydroxycoumarin

168    fluorescence was measured in a PerkinElmer LS 50B luminescence

169    spectrophotometer, using an excitation wavelength of 332 nm and emission

170    wavelength at 456 nm [21]. The excitation and emission slit width was 4 mm and the

171    scan rate was 200 nm/min. A sample UV/Visible and fluorimeter spectra, with peaks at

172    277 nm and 456 nm respectively, are shown in the supplementary material Figure S2

173    and Figure S3. All experiments were performed in triplicate.

174

175    **2.4  OH radical quantification**

176        OH radicals were quantified based on a modified method described by Zhang *et al.*

177    [38] and according to equation 1. The concentration of OH radicals was calculated by

178    assuming that 6.1 % of total OH radicals were captured as 7-hydroxycoumarin. The

179    stoichiometric ratio of one mole of OH radical consumed for the production of one mole

180    of 7-hydroxycoumarin was used [23]. The total number of OH radicals produced over

181    time during this photocatalytic process was calculated using the following equation.

182

183     $X = \{\frac{A}{6.1\%} - B\}$       ............................................................... Equation 1

184

185     Where, X is the total OH radical concentration (µM) produced during photocatalysis, A

186     is the mean 7-hydroxycoumarin concentration (µM) and B is the amount of OH radicals

187     (µM) produced during the light control experiments. The concentration of coumarin and

188     7-hydroxycoumarin was calculated using a standard curve of known concentrations as

189     shown in the supplementary material (Figure S4, Figure S5 and Figure S6).

190

191     **3.    RESULTS AND DISCUSSION**

192     **3.1 Characterisation of Photocatalysts**

193       XRD patterns of $WO_3$, $Cr-SrTiO_3$ and $LaCr-SrTiO_3$ samples were determined as

194     shown (Figure 1). The commercial $WO_3$ nanoparticles exhibited a typical crystallized

195     monoclinic phase structure, and the Cr-doped and La,Cr-co-doped $SrTiO_3$ samples

196     possessed homogeneous crystallized cubic perovskite structures, with no impurity

197     phase found for either of the doped samples and these results were consistent with

198     literature [44,45]. In the co-doped samples, since La and Cr substitute the Sr and Ti,

199     respectively, and the radius of La is similar with that of Sr while the radius of Cr was

200     similar to that of Ti, the peak positions of the $Cr-SrTiO_3$ and $LaCr-SrTiO_3$ samples are

201     not shifted compared to those of pure $SrTiO_3$.

202

203     **Figure 1.**

204

205       In the UV−visible absorption spectra of $WO_3$, $Cr-SrTiO_3$ and $LaCr-SrTiO_3$ (Figure

206     2), $WO_3$ exhibited visible light absorption up to 470 nm, which corresponds to the band-

207     gap energy of ca. 2.64 eV. $SrTiO_3$, however, has no absorption in the visible light

208     region (bandgap of 3.75 eV) and metal-doping has been shown to be a feasible

209     method for extending the light absorption of $SrTiO_3$ into the visible region [46]. Doping

210  of Cr into the A-site of $SrTiO_3$ induces an absorption band in the visible region centred

211  at around 450 nm (Figure 2). The visible light absorption is ascribed to the electron

212  excitation from the Cr doping levels formed above the valence band of $SrTiO_3$ to the

213  conduction band of $SrTiO_3$ [43]. It was reported that La, Cr- co-doped $SrTiO_3$ showed

214  enhanced photocatalytic performance compared to the single Cr-doped $SrTiO_3$ due to

215  the inhibition of the formation of $Cr^{6+}$ species in the B site [43]. Therefore, a co-doped

216  sample, LaCr-$SrTiO_3$ was prepared by the same method. The visible light absorption of

217  LaCr-$SrTiO_3$ was significantly enhanced compared to the Cr-$SrTiO_3$, with two strong

218  absorption peaks centred at around 450 nm and 650 nm in the visible light region. In

219  the case of co-doping, more intermittent doping levels are formed within the band-gap

220  of $SrTiO_3$ compared to the single Cr doped $SrTiO_3$, which results in the visible light

221  absorption.

222

223  **Figure 2.**

224

225  **3.2  Photocatalytic OH radical production**

226  **3.2.1   UV light photocatalysis on P25**

227  P25 has been one of the most extensively investigated and most active

228  commercially available photocatalysts under UV irradiation and therefore was used as

229  a benchmark for comparison in this study. Although, recent studies have reported that

230  nano-spherical $InCrO_4$-loaded $TiO_2$ and $TiO_2$ nanospheres deposited on graphene

231  performed better than P25 for OH radical production and dye degradation upon UV

232  irradiation [47,48], to date P25 is still regarded as the benchmark. The photocatalytic

233  hydroxylation of coumarin over P25 under UV light and subsequent formation of 7-

234  hydroxycoumarin is shown in Figure 3. The production of 7-hydroxycoumarin under

235  these conditions equates to a peak OH radical concentration of 16.9 µM after 45 mins.

236

9

237     **Figure 3.**

238     As shown in the figure, near complete degradation (97 %) of coumarin was

239     achieved after 120 mins irradiation. This level of degradation was likely to result from

240     the increased adsorption of coumarin onto the catalyst, which facilitated the reaction

241     with surface bound OH radicals. The role of surface bound radicals and those that are

242     present in bulk has been highlighted in a previous publication by Li *et al.* [49], who

243     investigated acid orange oxidation over $TiO_2$ P25 and AgBr. This group investigated

244     the quenching of OH radicals at the catalyst surface and in bulk in order to demonstrate

245     that surface bound species were the predominant radicals in the oxidation pathway.

246     This observation confirmed that increased adsorption of the substrate on the catalyst

247     surface can significantly increase the degradation efficiency.

248

249     Figure 3 also shows the profile of 7-hydroxycoumarin production and

250     decomposition which indirectly indicates the quantity of OH radicals generated. 7-

251     hydroxycoumarin concentration peaked at 45 minutes, with a maximum concentration

252     of 1.045 µM, which was equivalent to 16.9 µM OH radicals (as calculated from

253     equation 1). It was observed that an average production rate of 1.8 µM/hr was

254     achieved during the first 45 mins, followed by an average degradation rate of 0.46

255     µM/hr during the latter stages of irradiation. The decrease in concentration of 7-

256     hydroxycoumarin could also be attributed to the presence of superoxide radicals as

257     reported by Czili and Horvath [23].

258

259     Several reports have suggested the kinetics for 7-hydroxycoumarin generation

260     from coumarin with P25 under UV irradiation are zero order [21,23,38,50-52], however,

261     a number of these investigations also used a high concentration of both catalyst and

262     coumarin. Furthermore, it has been suggested that at higher concentrations of

263     coumarin (>100 µM), more UV light is absorbed by this probe and not the catalyst,

which results in a low 7-hydroxycoumarin and OH radical production rate [23]. In the present study, $K_{app}$ which is the rate constant for the formation of 7-hydroxycoumarin was calculated to be 0.0234 µM/min whereas $K_{dis}$, the rate constant for the disappearance of 7-hydroxycoumarin was calculated to be 0.0135 µM/min. In this study we have established that both, production and degradation of 7-hydroxycoumarin followed zero order kinetics, which is agreement with previous studies.

### 3.2.2   Visible light photocatalysis

A number of visible light catalysts were also selected for comparison against P25 $TiO_2$. While the synthesised catalysts all possessed energy band gaps that supported visible light activation, only $WO_3$ and $Pt-C_3N_4$ had energy band potentials (valence band at 3.2 V and 1.4 V respectively and conduction band at 0.2 V and -1.3 V respectively) that would facilitate OH radical formation either directly or indirectly as mentioned in reactions 2–6. Catalysts $LaCr-SrTiO_3$, $Cr-SrTiO_3$ and yellow $TiO_2$ (valence bands at 2.7 V, 2.7 V and 2.6 V respectively and conduction bands at -0.1 V for all the three photocatalysts) were selected to monitor if 7-hydroxycoumarin was formed even when the electronic structure of the catalyst was not suited to the redox potential of the reaction.

The photocatalytic hydroxylation of coumarin to 7-hydroxycoumarin over $WO_3$ and $Pt-C_3N_4$ under visible light is shown in Figure 4. As can be seen, minimal conversion of coumarin was observed over both $Pt-C_3N_4$ and $WO_3$, which was also supported by the low formation of 7-hydroxycoumarin (Figure 5). $Pt-C_3N_4$ displayed a slow yet steady conversion rate, reaching a 0.91 % drop in coumarin after 120 mins of irradiation whereas, a varying coumarin concentration pattern was seen over time on $WO_3$. It is interesting to note that there was an initial decrease in coumarin concentration followed by an increase which may be attributed to coumarin desorption from the surface of

11

291    WO$_3$. This desorption could be a result of the alteration in equilibrium in the closed

292    system due to the possible evolution of O$_2$ from water on WO$_3$ under visible light.

293

294    **Figure 4.**

295

296    While the decrease in coumarin concentration is low, production of OH radicals

297    over Pt-C$_3$N$_4$ and WO$_3$ was supported by the detection of 7-hydroxycoumarin upon

298    photocatalysis (Figure 5). When WO$_3$ was used as the photocatalyst, there was no 7-

299    hydroxycoumarin production until 30 minutes of irradiation which could be due to the

300    rapid recombination of the electrons and the photo generated holes. After 30 minutes,

301    OH radical production was steady with a gradual generation of 7-hydroxycoumarin

302    being observed. In the case of Pt-C$_3$N$_4$ however, 7-hydroxycoumarin production was

303    seen from 15 minutes.  The initial increase in the 7-hydroxycoumarin concentration

304    correlates to a rapid degradation of coumarin during the first 60 mins of irradiation.

305

306    **Figure 5**.

307

308    In contrast to Pt-C$_3$N$_4$ and WO$_3$, the catalysts LaCr-SrTiO$_3$, Cr-SrTiO$_3$ and yellow

309    TiO$_2$ displayed no activity towards coumarin conversion to 7-hydroxycoumarin, which

310    indicates no OH radical formation. Furthermore, under prolonged visible light irradiation

311    no detectable 7-hydroxycoumarin was recorded.

312

313    **3.2.3   Influence of photocatalysts' electronic structure and particle size on OH**

314        **radical formation**

315    In order to evaluate and discuss the performance of the catalysts, it is essential to

316    consider the primary contributing factors; electronic structure and particle size. The

317    electronic structure of the catalysts dictates the initial photo-excitation of electrons to

318 higher energy levels, while the particle size dictates the concentration of photons

319 absorbed and surface reactions between coumarin and OH radicals. As shown in

320 reactions (2) – (6), OH radicals can occur via two routes in photocatalysis. The direct

321 formation at the valence band requires a redox potential of 2.8 V vs NHE, while the

322 indirect method occurs via the intermediate radical, $O_2^{-}$ and requires a redox potential

323 of -0.33 V vs NHE [53]. The electronic structure of the catalysts tested in this study, in

324 relation to the redox potentials required for radical formation, are shown in Figure 6.

325

326 **Figure 6**

327

328 As Figure 6 shows, catalysts $TiO_2$ P25, $Pt-C_3N_4$ and $WO_3$ possess an electronic

329 structure which corresponds to the redox potential of OH radical formation via either

330 direct or indirect mechanisms. The favourable electronic structure of $TiO_2$ for OH

331 radical formation has been well documented and is evident from the results highlighted

332 here. The performance of $Pt-C_3N_4$ and $WO_3$ for OH radical formation, however, has not

333 been as well reported. The structure of $WO_3$ with a more positive valence band

334 suggests it is capable of generating surface OH radicals, however, the results obtained

335 indicate minimal 7-hydroxycoumarin production within 2 hours. Based on the structure,

336 it was likely an increased rate of recombination preventing OH radical formation via the

337 valence band hole, due to insufficient energy to initiate a reduction reaction at the

338 conduction band [21]. To prevent recombination and to increase the OH radical

339 production, Kim *et al*. synthesised Pt-doped $WO_3$ and found that the OH radical

340 production from $Pt-WO_3$ was significantly higher than un-doped $WO_3$ [20]. Furthermore,

341 the large particle size of approximately 100 nm for $WO_3$ indicates a smaller surface

342 area, which leads to minimum absorption of light.

343

344    The electronic structure of Pt-$C_3N_4$ as seen from Figure 6 clearly indicates a

345    reducing catalyst, which is also supported by its application in water reduction

346    investigations [54]. Therefore, the hydroxylation of coumarin and subsequent formation

347    of 7-hydroxycoumarin, as indicated by the earlier results, is likely via the indirect $O_2^-$

348    pathway. Based upon this observation, it is likely the low yield of OH radicals is a result

349    of competition for the conduction band electron between superoxide formation and $H^+$

350    reduction to form $H_2$ (0 V vs NHE). In addition, since all these experiments were

351    performed in a closed system with limited $O_2$, a reducing catalyst such as Pt-$C_3N_4$ is

352    expected to produce less OH radicals than an open system. Furthermore, despite a

353    favourable particle size of 20-40 nm, Pt-$C_3N_4$ was observed to agglomerate to form

354    larger aggregates leading to a decrease in surface area and in turn light absorption.

355

356    In the case of LaCr-$SrTiO_3$, Cr-$SrTiO_3$ and yellow $TiO_2$, the electronic structures

357    showed both the valence band and conduction band of all these catalysts to be lower

358    than the redox potentials to facilitate radical formation as seen in Figure 6. These

359    catalysts were primarily used as a control parameter to ensure no 7-hydroxycoumarin

360    formation was observed.

361

362    The calculated OH radical concentrations and production rates produced over all

363    catalysts screened are summarised in Table 1. The results show that the activity of the

364    visible light activated photocatalysts studied were significantly lower than commercial

365    P25 under UV light. This further emphasises that although there are numerous visible

366    light absorbing photocatalysts, their ability to produce OH radicals is significantly lower

367    than P25. In future, if any visible light absorbing photocatalysts are to be fabricated for

368    the purpose of photocatalytic oxidation, their OH radical producing rates (and

369    quantities) should be determined and compared to P25 as demonstrated here.

370

371    **Table 1**

372

373    **4.    CONCLUSION**

374    The aim of screening UV and visible light absorbing photocatalysts to assess their

375    oxidative strength was accomplished successfully by trapping OH radicals produced by

376    the photocatalysts in 7-hydroxycoumarin. The OH radical production capabilities of

377    various photocatalysts covering a range of band gaps and particle sizes were assessed

378    by comparing and discussing their differences with the commercial UV light activated

379    P25.  To conclude, visible light activated photocatalysts such as LaCr-SrTiO$_3$, Cr-

380    SrTiO$_3$ and yellow TiO$_2$ did not produce any OH radicals and this could be attributed to

381    their electronic structure. Whereas, the (pseudo) maximum OH radical production rates

382    of other visible light activated photocatalysts namely, WO$_3$ (0.28 μM/hr) and Pt-C$_3$N$_4$

383    (0.886 μM/hr) were found to be significantly lower when compared to the commercial

384    UV light activated P25 photocatalyst (35.654 μM/hr). This method could be further

385    exploited as novel photocatalysts are developed and to compare a range of P25

386    concentrations for OH radical production. This study further emphasises the challenges

387    faced by the visible light photocatalysts for photocatalytic oxidation.

388

397

## REFERENCES

[1] A. Fujishima, K. Honda, Electrochemical Photolysis of Water at a Semiconductor Electrode, Nature. 238 (1972) 37-38.

[2] D.W. Bahnemann, L.A. Lawton, P.K.J. Robertson, The Application of Semiconductor Photocatalysis for the Removal of Cyanotoxins from Water and Design Concepts for Solar Photocatalytic Reactors for Large Scale Water Treatment, in: S.L. Suib (Ed.), New and Future Developments in Catalysis, 1st ed., Elsevier, Amsterdam, 2013, pp. 395-415.

[3] M.R. Hoffmann, S.T. Martin, W. Choi, D.W. Bahnemann, Environmental Applications of Semiconductor Photocatalysis, Chem. Rev. 95 (1995) 69-96.

[4] P.K.J. Robertson, J.M.C. Robertson, D.W. Bahnemann, Removal of microorganisms and their chemical metabolites from water using semiconductor photocatalysis, J. Hazard. Mater. 211–212 (2012) 161-171.

[5] H. Kominami, S. Murakami, M. Kohno, Y. Kera, K. Okada, B. Ohtani, Stoichiometric decomposition of water by titanium(IV) oxide photocatalyst synthesized in organic media: Effect of synthesis and irradiation conditions on photocatalytic activity, Phys. Chem. Chem. Phys. 3 (2001) 4102-4106.

[6] C. McCullagh, P.K.J. Robertson, M. Adams, P.M. Pollard, A. Mohammed, Development of a slurry continuous flow reactor for photocatalytic treatment of industrial waste water, J. Photochem. Photobiol. A. 211 (2010) 42-46.

[7] P.K.J. Robertson, Semiconductor photocatalysis: an environmentally acceptable alternative production technique and effluent treatment process, J. Clean. Prod. 4 (1996) 203-212.

[8] M. Adams, I. Campbell, C. McCullagh, D. Russell, D.W. Bahnemann, P.K.J. Robertson, From Ideal Reactor Concepts to Reality: The Novel Drum Reactor for Photocatalytic Wastewater Treatment, Int. J. Chem. React. Eng. 11 (2013) 621-632.

[9] O. Carp, C.L. Huisman, A. Reller, Photoinduced reactivity of titanium dioxide, Progress in Solid State Chemistry. 32 (2004) 33-177.

[10] C. McCullagh, N. Skillen, M. Adams, P.K.J. Robertson, Photocatalytic reactors for environmental remediation: a review, J. Chem. Technol. Biotechnol. 86 (2011) 1002-1017.

[11] J. Jiang, Z. Zhou, V.K. Sharma, Occurrence, transportation, monitoring and treatment of emerging micro-pollutants in waste water — A review from global views, Microchem. J. 110 (2013) 292-300.

[12] A. Asghar, A.A. Abdul Raman, W.M.A. Wan Daud, Advanced oxidation processes for in-situ production of hydrogen peroxide/hydroxyl radical for textile wastewater treatment: a review, J. Clean. Prod. 87 (2015) 826-838.

435    [13] H. Fan, G. Li, F. Yang, L. Yang, S. Zhang, Photodegradation of cellulose under UV
436    light catalysed by TiO2, J. Chem. Technol. Biotechnol. 86 (2011) 1107-1112.

437    [14] E. Szabó-Bárdos, K. Somogyi, N. Törő, G. Kiss, A. Horváth, Photocatalytic
438    decomposition of l-phenylalanine over TiO2: Identification of intermediates and the
439    mechanism of photodegradation, Appl. Catal. B: Environ. 101 (2011) 471-478.

440    [15] T. Hirakawa, K. Yawata, Y. Nosaka, Photocatalytic reactivity for O2− and OH
441    radical formation in anatase and rutile TiO2 suspension as the effect of H2O2 addition,
442    Appl. Catal. A-Gen. 325 (2007) 105-111.

443    [16] Y. Nosaka, T. Daimon, A.Y. Nosaka, Y. Murakami, Singlet oxygen formation in
444    photocatalytic TiO2 aqueous suspension, Phys. Chem. Chem. Phys. 6 (2004) 2917-
445    2918.

446    [17] X. Yan, T. Ohno, K. Nishijima, R. Abe, B. Ohtani, Is methylene blue an appropriate
447    substrate for a photocatalytic activity test? A study with visible-light responsive titania,
448    Chemical Physics Letters. 429 (2006) 606-610.

449    [18] B. Ohtani, Preparing Articles on Photocatalysis—Beyond the Illusions,
450    Misconceptions, and Speculation, Chem. Lett. 37 (2008) 216-229.

451    [19] A. Mills, An overview of the methylene blue ISO test for assessing the activities of
452    photocatalytic films, Applied Catalysis B: Environmental. 128 (2012) 144-149.

453    [20] J. Kim, C.W. Lee, W. Choi, Platinized WO3 as an Environmental Photocatalyst that
454    Generates OH Radicals under Visible Light, Environ. Sci. Technol. 44 (2010) 6849-
455    6854.

456    [21] Q. Xiang, J. Yu, P.K. Wong, Quantitative characterization of hydroxyl radicals
457    produced by various photocatalysts, J. Colloid Interface Sci. 357 (2011) 163-167.

458    [22] M. Sato, T. Ohgiyama, J.S. Clements, Formation of chemical species and their
459    effects on microorganisms using a pulsed high voltage discharge in water, Industry
460    Applications Society Annual Meeting. 2 (1994) 1455-1461.

461    [23] H. Czili, A. Horváth, Applicability of coumarin for detecting and measuring hydroxyl
462    radicals generated by photoexcitation of TiO2 nanoparticles, Appl. Catal. B: Environ. 81
463    (2008) 295-302.

464    [24] R. Ono, T. Oda, Measurement of hydroxyl radicals in pulsed corona discharge, J.
465    Electrostatics. 55 (2002) 333-342.

466    [25] W. Hoeben, E. van Veldhuizen, W. Rutgers, G. Kroesen, Gas phase corona
467    discharges for oxidation of phenol in an aqueous solution, J. Phys. D: Appl. Phys. 32
468    (1999) 133-137.

469    [26] P. Sunka, V. Babický, M. Clupek, P. Lukes, M. Simek, J. Schmidt, M. Cern,
470    Generation of chemically active species by electrical discharges in water, Plasma
471    Sources Sci. Technol. 8 (1999) 258-265.

472    [27] B. Sun, M. Sato, J. Sid Clements, Optical study of active species produced by a
473    pulsed streamer corona discharge in water, J. Electrostatics. 39 (1997) 189-202.

474    [28] M.G. Steiner, C.F. Babbs, Quantitation of the hydroxyl radical by reaction with
475    dimethyl sulfoxide, Arch. Biochem. Biophys. 278 (1990) 478-481.

476    [29] M. Sahni, B.R. Locke, Quantification of Hydroxyl Radicals Produced in Aqueous
477    Phase Pulsed Electrical Discharge Reactors, Ind. Eng. Chem. Res. 45 (2006) 5819-
478    5825.

479    [30] J. Ku, E. Zimowski,  United States Department of Labor, Occupational Safety and
480    Health Administration. 3M Formaldehyde Monitor (Model 3721), Product evaluation
481    (PE-10). 205 (1989).

482    [31] S.A.V. Eremia, D. Chevalier-Lucia, G. Radu, J. Marty, Optimization of hydroxyl
483    radical formation using TiO2 as photocatalyst by response surface methodology,
484    Talanta. 77 (2008) 858-862.

485    [32] T. Maezono, M. Tokumura, M. Sekine, Y. Kawase, Hydroxyl radical concentration
486    profile in photo-Fenton oxidation process: Generation and consumption of hydroxyl
487    radicals during the discoloration of azo-dye Orange II, Chemosphere. 82 (2011) 1422-
488    1430.

489    [33] M. Tokumura, R. Morito, R. Hatayama, Y. Kawase, Iron redox cycling in hydroxyl
490    radical generation during the photo-Fenton oxidative degradation: Dynamic change of
491    hydroxyl radical concentration, Appl. Catal. B: Environ. 106 (2011) 565-576.

492    [34] S. Kanazawa, T. Furuki, T. Nakaji, S. Akamine, R. Ichiki, Measurement of OH
493    Radicals in Aqueous Solution Produced by Atmospheric-pressure LF Plasma Jet, I. J.
494    PEST. 6 (2012) 166-171.

495    [35] K. Ishibashi, A. Fujishima, T. Watanabe, K. Hashimoto, Quantum yields of active
496    oxidative species formed on TiO2 photocatalyst, J. Photochem. Photobiol. A. 134
497    (2000) 139-142.

498    [36] T. Hirakawa, Y. Nosaka, Properties of O2.- and OH. Formed in TiO2 Aqueous
499    Suspensions by Photocatalytic Reaction and the Influence of H2O2 and Some Ions,
500    Langmuir. 18 (2002) 3247-3254.

501    [37] Z. Li, T. Liang, S. Lv, Q. Zhuang, Z. Liu, A Rationally Designed Upconversion
502    Nanoprobe for in Vivo Detection of Hydroxyl Radical, J. Am. Chem. Soc. 137 (2015)
503    11179-11185.

504    [38] J. Zhang, Y. Nosaka, Quantitative Detection of OH Radicals for Investigating the
505    Reaction Mechanism of Various Visible-Light TiO2 Photocatalysts in Aqueous
506    Suspension, J. Phys. Chem. C. 117 (2013) 1383-1391.

507    [39] M.E. Lindsey, M.A. Tarr, Quantitation of hydroxyl radical during Fenton oxidation
508    following a single addition of iron and peroxide, Chemosphere. 41 (2000) 409-417.

509 [40] J. Zhang, Y. Nosaka, Generation of OH radicals and oxidation mechanism in
510 photocatalysis of WO3 and BiVO4 powders, J. Photochem. Photobiol. A. 303–304
511 (2015) 53-58.

512 [41] F. Fina, H. Menard, J.T.S. Irvine, The effect of Pt NPs crystallinity and distribution
513 on the photocatalytic activity of Pt-g-C3N4, Phys. Chem. Chem. Phys. 17 (2015)
514 13929-13936.

515 [42] C. Randorn, J.T.S. Irvine, P. Robertson, Synthesis of Visible-Light-Activated
516 Yellow Amorphous Photocatalyst, Int. J. Photoenergy. 2008 (2008) 1-6.

517 [43] S. Ouyang, H. Tong, N. Umezawa, J. Cao, P. Li, Y. Bi, Y. Zhang, J. Ye, Surface-
518 Alkalinization-Induced Enhancement of Photocatalytic H2 Evolution over SrTiO3-Based
519 Photocatalysts, J. Am. Chem. Soc. 134 (2012) 1974-1977.

520 [44] M. Muralidharan, V. Anbarasu, A. Elaya Perumal, K. Sivakumar, Carrier mediated
521 ferromagnetism in Cr doped SrTiO3 compounds, J. Mater. Sci. : Mater. Electron. 26
522 (2015) 6352-6365.

523 [45] J. Guo, Y. Li, S. Zhu, Z. Chen, Q. Liu, D. Zhang, W. Moon, D. Song, Synthesis of
524 WO3@Graphene composite for enhanced photocatalytic oxygen evolution from water,
525 RSC Adv. 2 (2012) 1356-1363.

526 [46] K. van Benthem, C. Elsässer, R.H. French, Bulk electronic structure of SrTiO3:
527 Experiment and theory, J. Appl. Phys. 90 (2001) 6156-6164.

528 [47] J. Kamalakkannan, V.L. Chandraboss, S. Prabha, S. Senthilvelan, Advanced
529 construction of heterostructured InCrO4-TiO2 and its dual properties of greater UV-
530 photocatalytic and antibacterial activity, RSC Adv. 5 (2015) 77000-77013.

531 [48] M. Wojtoniszak, B. Zielinska, R.J. Kalenczuk, E. Mijowska, Photocatalytic
532 performance of titania nanospheres deposited on graphene in coumarin oxidation
533 reaction, Materials Science-Poland. 30 (2012) 32-38.

534 [49] G. Li, K.H. Wong, X. Zhang, C. Hu, J.C. Yu, R.C.Y. Chan, P.K. Wong, Degradation
535 of Acid Orange 7 using magnetic AgBr under visible light: The roles of oxidizing
536 species, Chemosphere. 76 (2009) 1185-1191.

537 [50] J. Zhang, Y. Nosaka, Mechanism of the OH Radical Generation in Photocatalysis
538 with TiO2 of Different Crystalline Types, J. Phys. Chem. C. 118 (2014) 10824-10832.

539 [51] H. Guan, L. Zhu, H. Zhou, H. Tang, Rapid probing of photocatalytic activity on
540 titania-based self-cleaning materials using 7-hydroxycoumarin fluorescent probe, Anal.
541 Chim. Acta. 608 (2008) 73-78.

542 [52] Z. Huang, Q. Sun, K. Lv, Z. Zhang, M. Li, B. Li, Effect of contact interface between
543 TiO2 and g-C3N4 on the photoreactivity of g-C3N4/TiO2 photocatalyst: (0 0 1) vs (1 0
544 1) facets of TiO2, Applied Catalysis B: Environmental. 164 (2015) 420-427.

545 [53] P.M. Wood, The potential diagram for oxygen at pH 7, Biochem. J. 253 (1988)
546 287-289.

547    [54] G. Zhang, Z. Lan, L. Lin, S. Lin, X. Wang, Overall water splitting by Pt/g-C3N4
548    photocatalysts without using sacrificial agents, Chem. Sci. 7 (2016) 3062-3066.

549

564

**Figure 1**

565

566

567

568

569

570

571 **Figure 2**

572

573

574

575

576

577

578

579 **Figure 3**

580

**Figure 4**

582

**Figure 5**

583

584

585

586

587

588

589

590

591

592

593

594

595

596
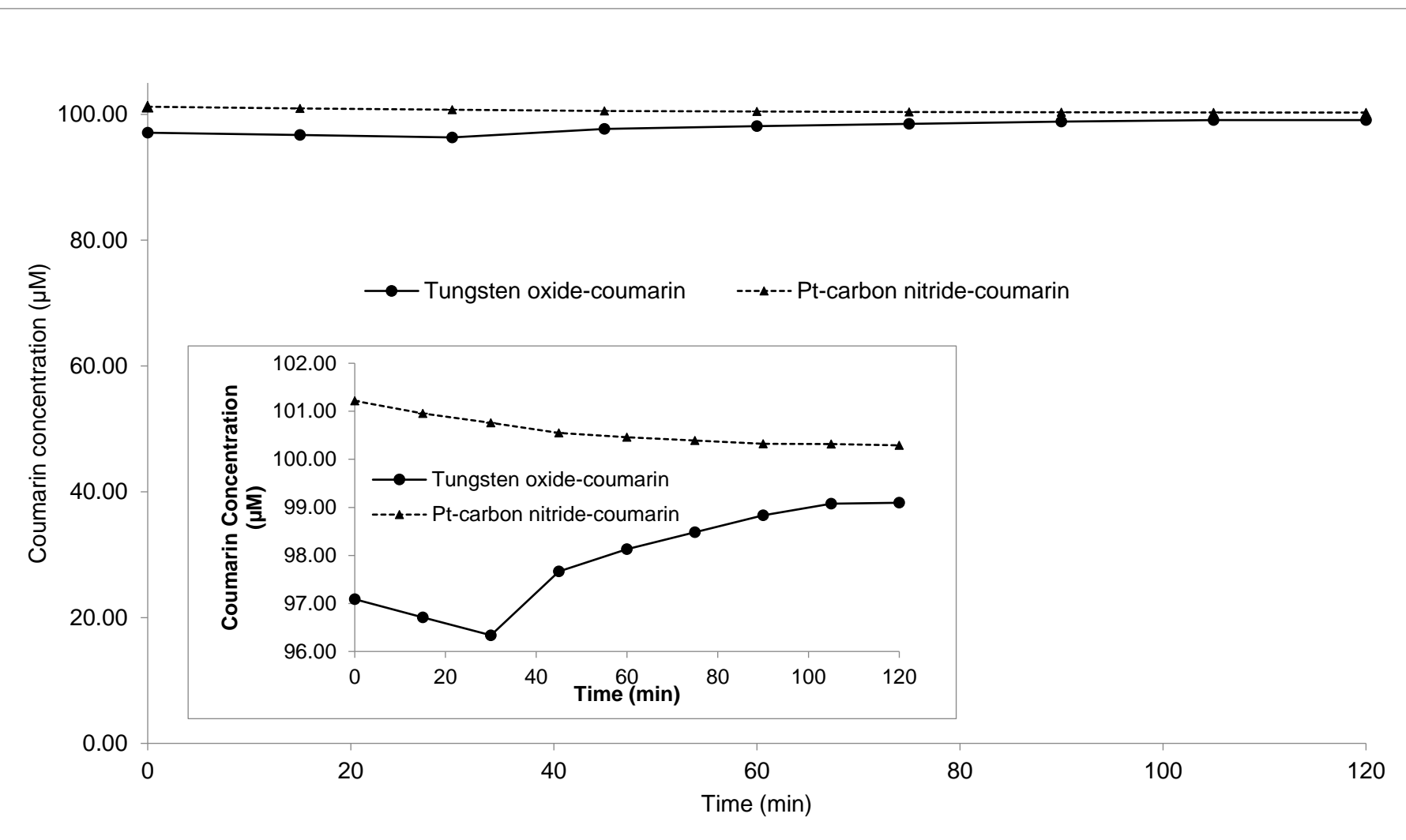
597

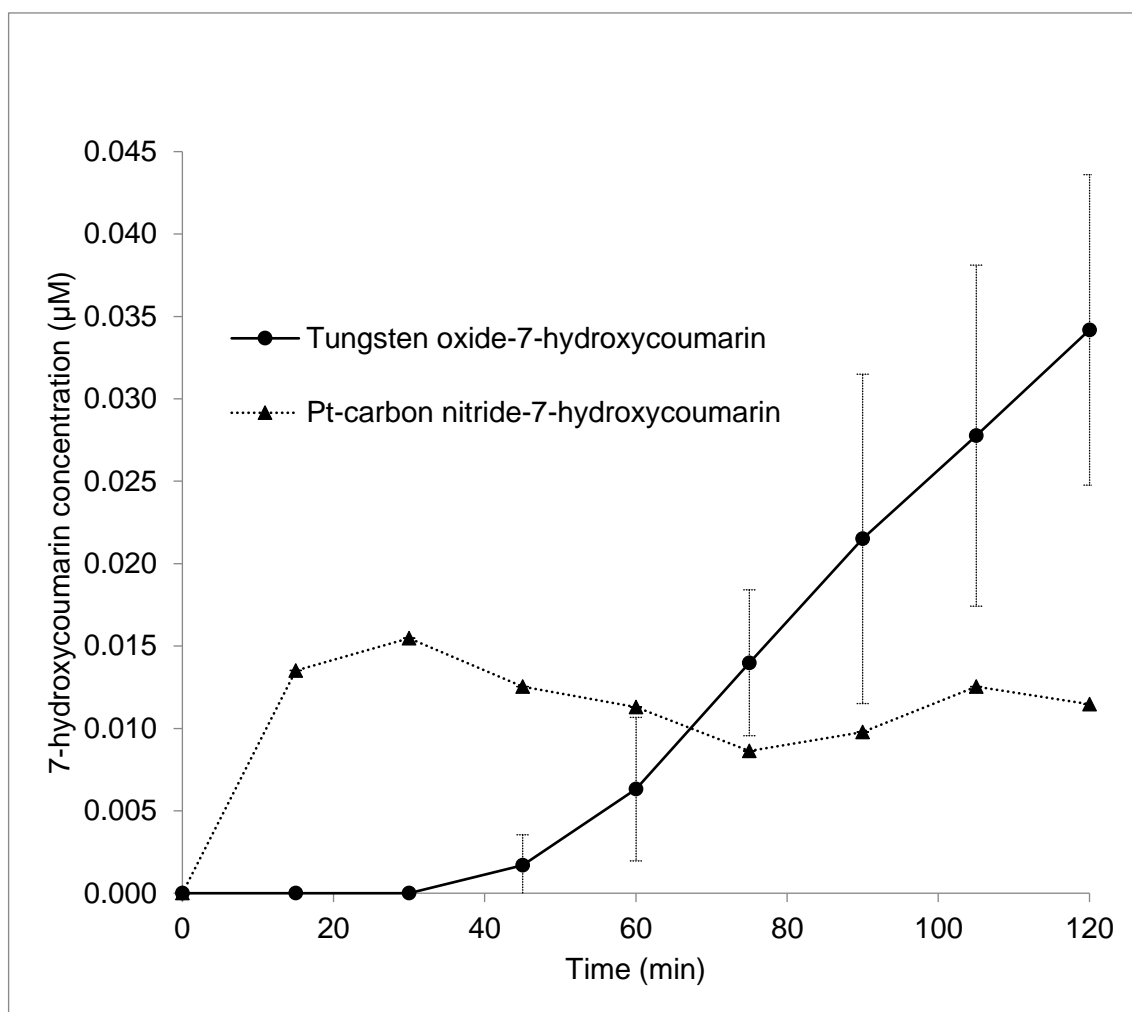598    **Figure 6**
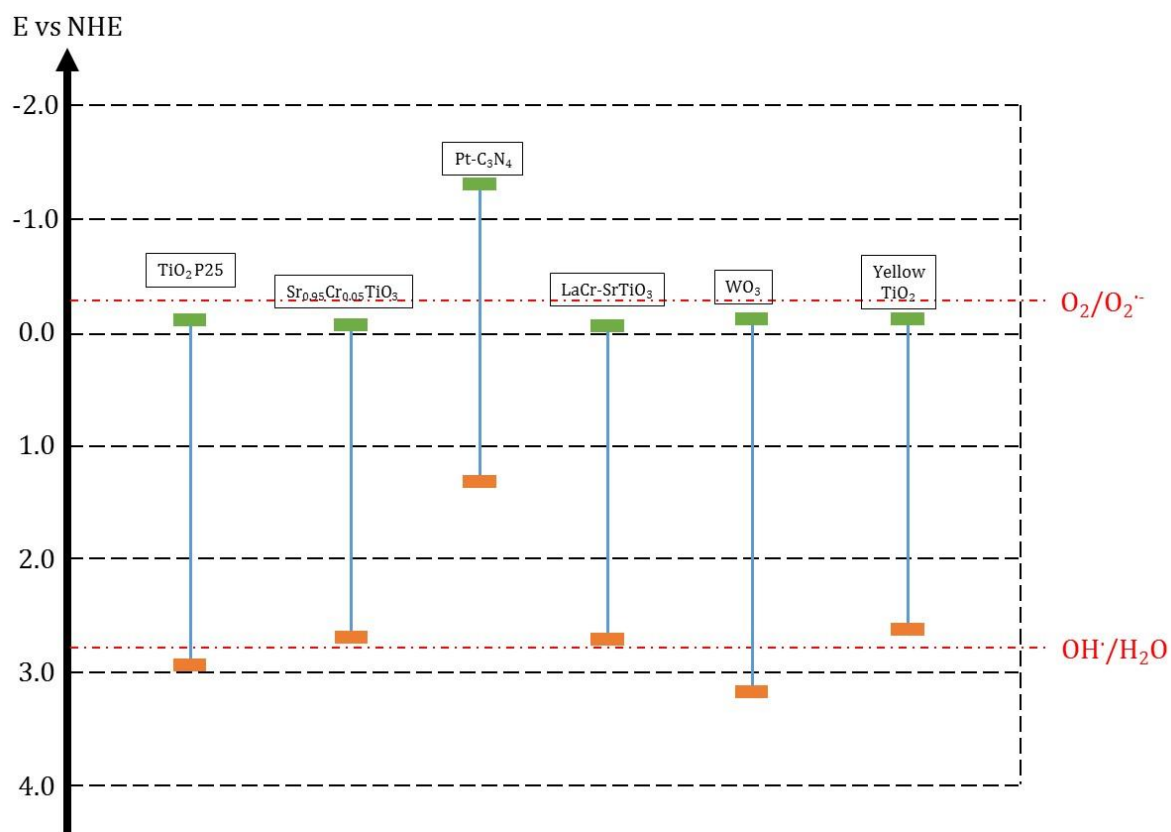
599

600

601

602

603

604

605

606

607

608

| Photocatalyst | Light Source | Maximum OH radical concentration (μM) | Time at which maximum concentration of OH radical was produced (min) | Maximum OH radical production rate (μM/hr) |
|---|---|---|---|---|
| P25 | UV | 16.9 | 45 | 35.654 |
| WO$_3$ | visible | 0.560 | 120 | 0.280 |
| Pt-C$_3$N$_4$ | visible | 0.254 | 30 | 0.886 |

609

610   **Table 1**